

## RESEARCH ARTICLE

# Structure and properties of bottlebrush polyelectrolyte complexes

Kaden C. Stevens  | Matthew V. Tirrell 

Pritzker School of Molecular Engineering,  
The University of Chicago, Chicago,  
Illinois, USA

## Correspondence

Matthew V. Tirrell, Pritzker School of  
Molecular Engineering, The University of  
Chicago, Chicago, IL 60637, USA.  
Email: [mtirrell@uchicago.edu](mailto:mtirrell@uchicago.edu)

## Funding information

Center for Hierarchical Materials Design,  
Grant/Award Number: 70NANB19H005

## Abstract

Structural variation of polyelectrolytes has been shown to play an important role in altering polyelectrolyte complex (PEC) properties in recent years. However, molecular-level details such as polyelectrolyte architecture remain underdeveloped. Here, we use a combination of ring-opening metathesis polymerization (ROMP), atom-transfer radical polymerization (ATRP), and postpolymerization reactions to create densely branched bottlebrushes of poly(dimethylamino ethyl methacrylate) and poly(tert-butyl methacrylate) with high molecular weights (MDa), which we then convert into fully charged and densely branched bottlebrushes of poly(trimethylaminoethyl methacrylate) (PTMAEMA) and poly(methacrylic acid) (PAA). We investigate the structure and properties of bottlebrush polyelectrolyte complexes (BPECs) using optical microscopy, rheology, cryogenic transmission electron microscopy (Cryo-TEM), and small-angle X-ray scattering (SAXS). Bottlebrush polyelectrolyte complexes are white solids, which exhibit gel-like mechanical properties, which we attribute to sidechain interpenetration. Using a combination of Cryo-TEM and SAXS, we are able to outline the structural development of BPECs, detailing how the network topology, sidechain conformation, and interdigitation spacing changes as a function of salt. Our results provide a foundation for further exploration of branched architectures within polyelectrolyte complexation.

## KEYWORDS

bottlebrushes, Cryo-TEM, polyelectrolyte complexes, polyelectrolytes, small-angle X-ray scattering

## 1 | INTRODUCTION

Mixing oppositely charged polyelectrolytes results in spontaneous associative phase separation and creates a polymer-rich phase known as a polyelectrolyte complex (PEC) that is responsive to unique stimuli such as pH, ionic strength, and temperature.<sup>1–6</sup> Polyelectrolyte complexes

have been used extensively in food products and cosmetics and are promising for applications in underwater adhesives, drug delivery, and nanoreactors.<sup>7–15</sup> The ability of PECs to create hydrated materials with properties ranging from glassy solids to viscous liquids makes them especially attractive as a materials platform.<sup>16,17</sup> However, it is still difficult to direct PEC properties through molecular design,

This is an open access article under the terms of the [Creative Commons Attribution](#) License, which permits use, distribution and reproduction in any medium, provided the original work is properly cited.

© 2023 The Authors. *Journal of Polymer Science* published by Wiley Periodicals LLC.

limiting the adoption of this promising class of materials. Early PEC studies utilized poorly defined natural polyelectrolytes, which exacerbated the difficulties associated with determining precise structure–property relationships. In recent years, synthetic techniques for growing well-defined water-soluble polymers have matured a great deal, enabling the synthesis of increasingly precise polyelectrolytes of various architectures.<sup>18,19</sup>

Despite the increasing availability of structurally advanced polyelectrolytes, the majority of PEC studies still utilize linear blocky, statistical, or homopolyelectrolytes.<sup>20–25</sup> As a result, there is a gap in our understanding of how molecular-level structural details such as polymer architecture influence PEC stability, rheology, and structure. Tuning PEC properties through tuning structural parameters of polyelectrolytes is an approach that has gained interest recently since the structure–property relationships obtained are generally conserved across various polyelectrolyte pairings and allow one to tune PEC properties without altering the surrounding environment.

Among structural parameters, charge density has emerged as a fundamental parameter in PEC design. In statistical copolymers, increased charge density has been shown to raise PEC stability and strengthen PEC mechanical properties.<sup>23,26,27</sup> Branched polyelectrolytes increase spatial charge density relative to linear polyelectrolytes, making them attractive candidates for further enhancement of PEC properties. However, there are no reports of altering charge density higher homopolyelectrolytes using branched polymers. To realize the promise of branched polyelectrolytes, macromolecular design is crucial.

The first published attempt at PECs from comb polyelectrolytes could not demonstrate comb–comb PECs due to insufficient charge density.<sup>28</sup> They attribute this result to their sparsely branched comb architecture with short sidechains. Simulations showed that these comb-like polyelectrolytes had lower spatial charge density than comparable linear counterparts, which reduced PEC stability. Here, we create charge dense bottlebrush polyelectrolytes by combining ring-opening metathesis polymerization (ROMP), atom-transfer radical polymerization (ATRP), and postpolymerization modification (PPM) reactions to understand the emergent properties of bottlebrush polyelectrolyte complexes (BPECs). We find that BPECs form solid precipitate complexes, which behave as mechanically arrested gels, a feature we attribute to physical crosslinks arising from sidechain interdigitation. Using a combination of small-angle X-ray scattering (SAXS) and cryogenic transmission electron microscopy (Cryo-TEM), we investigate the internal structure of BPECs and generate a unified picture of the structure and properties of BPECs as a function of sodium chloride concentration that will enable future exploration of branched polyelectrolytes in PECs.

## 2 | RESULTS AND DISCUSSION

### 2.1 | Bottlebrush polyelectrolyte synthesis

To create large, highly branched bottlebrush polyelectrolytes, we combined ROMP, ATRP, and PPM reactions. Our approach, adapted from Yamauchi et al., utilizes a grafting-from methodology centered around the monomer 2-endo, 3-endo-Bis(2-bromoisobutyryloxymethyl)-5-norbornene (NB), which serves as a ROMP monomer due to the norbornene functionality and as an initiator for ATRP due to the two pendant 2-bromoisobutylate moieties (Figure 1).<sup>29</sup> Ring-opening metathesis polymerization of NB proceeds rapidly to produce Poly(NB) (PNB) with narrow dispersity ( $\bar{D} = 1.01$ ) and predictable molecular weights (targeted DP = 300). From PNB, we graft neutral sidechains of poly(*tert*-butyl methacrylate) (PtBMA) and poly(dimethylamino ethyl methacrylate) (PDMAEMA) via ATRP (Figure 1B,C). Neutral sidechains are converted into polyelectrolytes through quantitative detertbutylation and quaternization reactions to form PNB-g-MANa and PNB-g-TMAEMA, respectively. For brevity, we will refer to the graft polymers PNB-g-MANa as PMANa and PNB-g-TMAEMA as TMAEMA<sub>X</sub> where X can be S or L for short or long sidechain TMAEMA. Two sidechain lengths of TMAEMA were made to evaluate the effect of chain length matching/mismatching, with the longer TMAEMA sidechains more closely matching the DP of the PMANa sidechains and the short TMAEMA sidechains having approximately half the DP of the longer TMAEMA sidechains (Figure 1C).

### 2.2 | PEC morphology and optical microscopy

Bottlebrush polyelectrolyte complex samples were prepared by sequentially mixing water, NaCl stock solutions, and polymers followed by rapid mixing. The turbid samples were then centrifuged to coalesce the BPEC phase for further studies. All BPECs were created using stock solutions of water, polymer, and salt titrated to pH 10, to account for the tendency of PMANa's pKa to shift upward at higher branching densities.<sup>30,31</sup> Previous reports show the pKa of carboxylic acid containing polyelectrolytes decreases when complexed with quaternary-amine containing polyelectrolytes, so we reason pH 10 should be sufficiently basic to ensure the PMANa groups are charged during complexation.<sup>24</sup>

Upon centrifugation to separate the complex and supernatant phase, the complex is observed to be a white

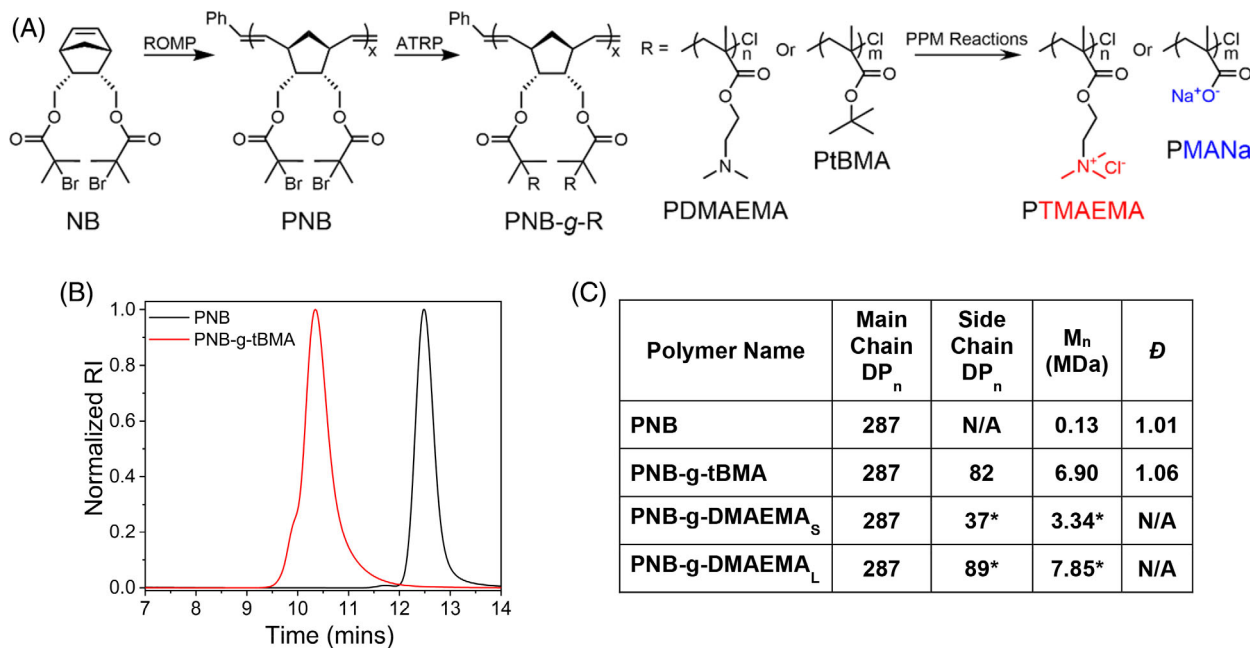


**FIGURE 1** (A) Scheme for bottlebrush polyelectrolyte synthesis. (B) GPC demonstrating conversion of macromonomer PNB into bottlebrush PNB-g-tBMA. (C) Table with molecular characterization of bottlebrushes. \*Estimated via  $^1\text{H}$  NMR.

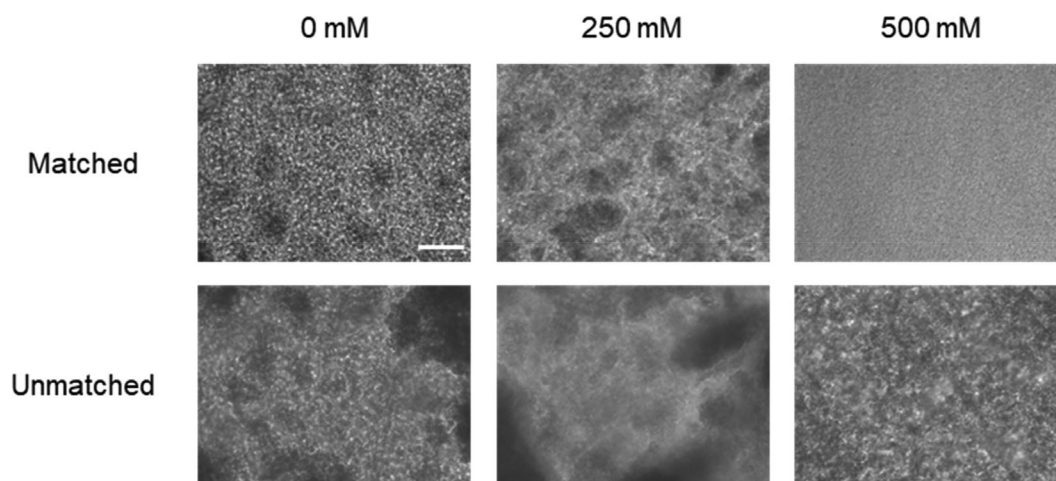


**FIGURE 2** Optical microscopy of bottlebrush polyelectrolyte complexes of PMANa and PTMAEMA with matched and unmatched sidechains as a function of added NaCl. Scale bar is 100  $\mu\text{m}$ .

solid (Figure S1). The complex swells with added salt, remaining white until around 400 mM added salt, where the BPEC becomes hazy. At 500 mM salt, the complex is nearly clear. No complex forms at higher salt concentrations. The macroscopic appearance of BPECs was identical for matched and mismatched sidechains.

We use optical microscopy to visualize BPECs at the microscale as a function of salt (Figure 2). Microscopy images showed the BPECs to be cloudy aggregates at all salt concentrations with a critical salt concentration (CSC) of 500 mM added NaCl. This microscale morphology indicates BPECs form solid-like precipitates or gels.

Interestingly, there is no transition from precipitate to coacervate before the CSC. In general, PECs transition from solid-like precipitates through liquid-like coacervates before dissolution. Here, however, the complex dissolves somewhere between 500 and 525 mM added NaCl, so the transition from solid to liquid complex must occupy an extremely narrow phase space if it exists at all. The microscale morphologies and CSC of BPECs at matched and mismatched sidechain lengths are indistinguishable. At all salt concentrations, all BPECs studied here appear as solid precipitates under optical microscopy.

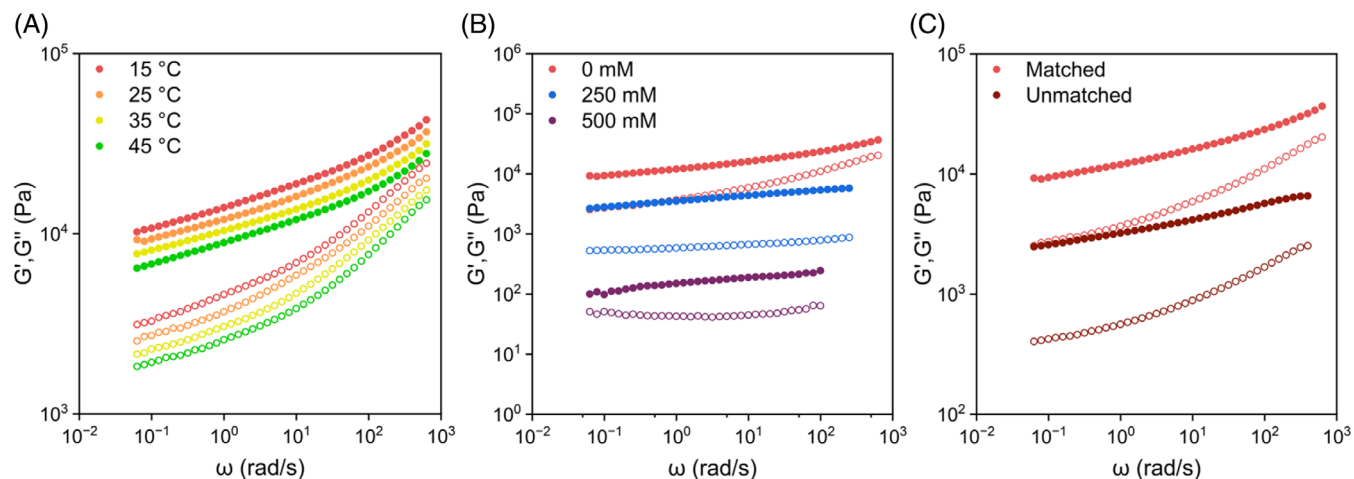


**FIGURE 3** Frequency sweeps for bottlebrush polyelectrolyte complexes with (A) 0 mM added NaCl at different temperatures (B) 0, 250, and 500 mM added NaCl at 25 °C and (C) matched or mismatched sidechain lengths.

## 2.3 | Rheology

Small-angle oscillatory shear (SAOS) experiments allowed us to further quantify the physical state and determine the stimuli-responsiveness of our materials. The BPECs show gel-like response with storage modulus ( $G'$ ) above loss modulus ( $G''$ ) at all frequencies, temperatures, and salt concentrations measured. With no added salt, our materials begin as soft gels, which further soften as salt is added, temperature is increased or sidechain length mismatch is increased (Figure 3). It was initially unclear why these materials are behaving as gels, as gel-like mechanical properties are normally observed in systems using relatively hydrophobic monomers capable of secondary interactions and prone to aggregation.<sup>17,32</sup>

Previous reports have observed gel-like rheological responses in PECs.<sup>17,32,33</sup> However, this feature is often attributed to aggregation at various length scales, usually driven by hydrophobic interactions between polyelectrolytes.<sup>17,33</sup> Here, we have no obvious source of hydrophobic interactions capable of inducing physical crosslinks, suggesting the gel-like behavior observed here is not caused by amphiphilic interactions within the system. There have been many reports of PECs made from very similar polyelectrolytes showing liquid-like viscoelastic behavior across a wide range of molecular weights.<sup>24,25,34,35</sup> Since it is unlikely that our rheological response is a result of the chemical composition of the polyelectrolytes we have chosen here, we speculate that gelation in our system is a result of the polyelectrolyte architecture. Strong intermolecular associations between interdigitated bottlebrush sidechains could restrict motion and act as physical crosslinks, which would be a novel mechanism for PEC gel formation. To fully understand the internal structure of PECs, we utilize Cryo-TEM and SAXS.

## 2.4 | Internal structure observation via Cryo-TEM

To better understand the internal structure of our gel-like BPEC, we performed Cryo-TEM experiments, reasoning that our bottlebrushes are long and densely branched enough to be imaged directly. To obtain clear images of PMANa, PTMAEMA<sub>L</sub>, and BPECs, we diluted the total polymer concentration to 0.5 mg/mL. Representative Cryo-TEM images of PMANa, PTMAEMA<sub>L</sub>, and BPECs are shown in Figure 4A.

Cryo-TEM images of the individual polyelectrolytes reveal densely branched polyelectrolytes with lengths on the order of 100 nm and widths of approximately 10–15 nm (Figures 4A, S4 and S5). The bottlebrushes are highly extended, which is expected due to the steric congestion and electrostatic repulsion between the densely grafted sidechains. The contrast is sufficient in the low salt case to allow us to estimate the bottlebrush thickness using ImageJ (Figure 4B). To the best of our knowledge, these are the first images of bottlebrush polyelectrolytes without external contrast agent.

With no added salt, the BPECs form densely packed structures with smooth surfaces. At this salt concentration, the BPECs exhibit dense interchain packing, with no discernible features attributable to individual polyelectrolytes. The BPEC surface is highly curved, which is surprising given the rigidity of the uncomplexed bottlebrush polyelectrolytes. The smooth, curved surfaces and densely packed structure of the low salt BPECs show polyelectrolyte complexation provides a strong driving force for association of oppositely charged bottlebrush sidechains in the absence of added salt, potentially perturbing the mainchain conformation of the constituent bottlebrushes within a BPEC significantly.



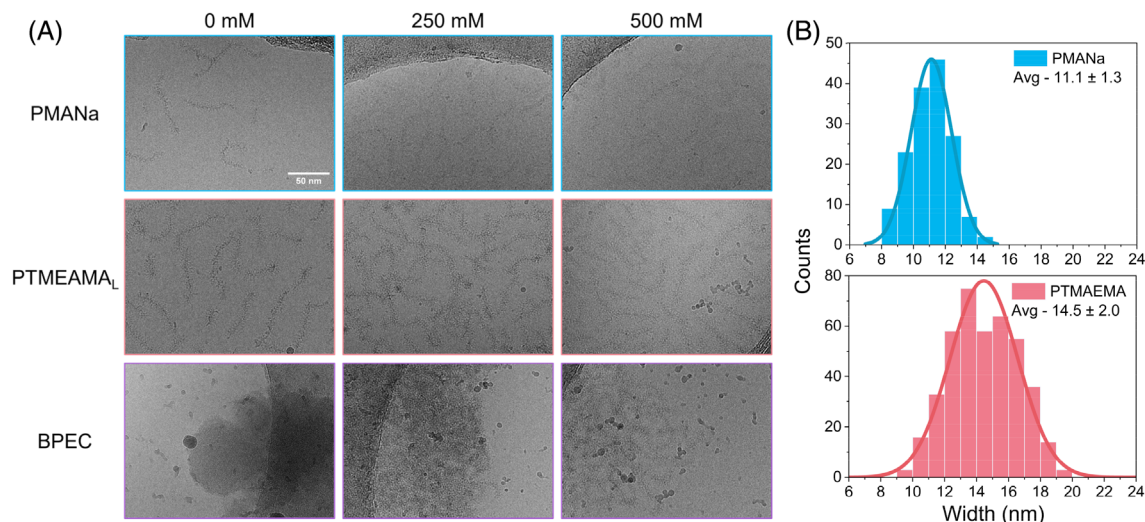


**FIGURE 4** (A) Cryo-TEM microscopy of bottlebrushes of PMANa and PTMAEMA<sub>L</sub> and bottlebrush polyelectrolyte complexes with matched sidechains as a function of added NaCl. Scale bar is 50 nm. (B) Histograms of bottlebrush width acquired via ImageJ analysis of 0 mM added salt bottlebrushes.

At 250 mM added salt, the BPEC swells and has rougher surfaces and an internal structure spaces in the complex are voids within the BPEC or thinner regions within the BPEC. Upon further examination, it appears that these are filled regions that are less densely packed than in the low salt case. This makes sense, as introducing salt is known to reduce the degree of intrinsic bonding between oppositely charged polymers, lowering the driving force for sidechain association.

At 500 mM added salt, the BPEC swells, becoming a swollen disordered network with no obvious surfaces (Figures 4A and S3). The bottlebrushes in this case are much more elongated than at other salt concentrations and connect at joints akin to crosslinks. These large, multivalent joints could be the physical crosslinks leading to gel-like rheological behavior in BPECs. If so, one can imagine how lowering salt would increase the joint density within the network and raise the modulus of the material in a manner analogous to crosslink density in traditional crosslinked polymer networks.

Mismatched complexes adopt similar structures to the matched complexes in Cryo-TEM, progressing as salt is added from a densely packed network to slightly swollen network before finally expanding into a filamentous network (Figure 5). It is difficult to detect differences in the mismatched and matched BPECs structures using Cryo-TEM alone.

To the best of our knowledge, these images provide the first look inside the structure of a pristine polyelectrolyte complex with molecular resolution. By growing tens of thousands of charged repeat units from a single main-chain, we synthesized polyelectrolytes significantly larger

and more compact than most studied in the literature. This novel arrangement of charged groups allows us to directly observe the individual polyelectrolytes and the network structure adopted bottlebrush polyelectrolytes upon complexation via Cryo-TEM. However, these images may not be representative of the BPEC structure upon centrifugation and only allow us to observe small sections of BPEC at a time. To better understand BPEC structure, we use the findings from Cryo-TEM to inform our interpretation of SAXS.

## 2.5 | Internal structure analysis via SAXS

To investigate the structure of our BPEC materials in the bulk, we performed synchrotron-based (SAXS) as a function of added NaCl (Figure 6). First, we will discuss the SAXS results from the length-matched pair in detail and then compare them with the structural trends for the mismatched case. In general, all samples show an upturn at low  $q$  ( $q < 0.01$ ), suggesting aggregation with  $R_g > 300$  nm (since the maximum observable  $R_g = 2\pi/q_{\min}$ ). At high  $q$  ( $q > 0.05$ ),  $I(q)$  as  $\sim q^{-1}$ , which we attribute to extended bottlebrush sidechains. Mid  $q$  ( $0.01 < q < 0.05$ ) features evolve as a function of added salt but can broadly be described as an  $R_g$  describing aspects of the bottlebrushes in every case except 0 mM added salt. At no added salt, the data are best described qualitatively, whereas the data for 100–500 mM added salt were amenable to model fitting via a shape-independent two-level Beaucage model fit.

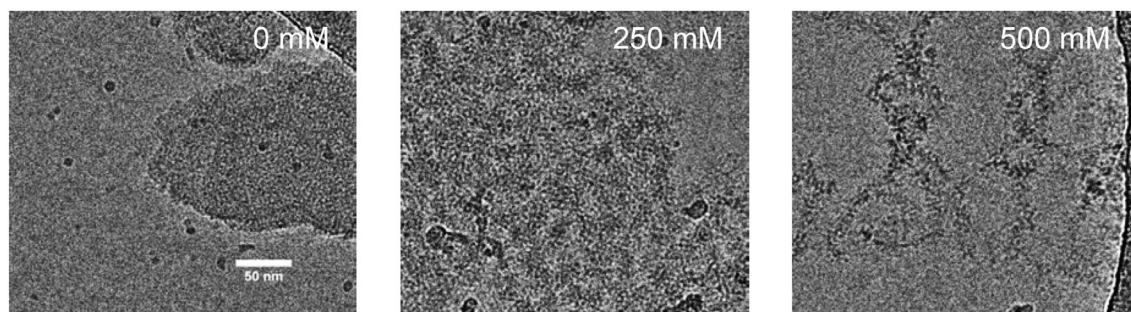


**FIGURE 5** Cryo-TEM microscopy of bottlebrush polyelectrolyte complexes with mismatched sidechains at 0, 250, and 500 mM added NaCl from left to right. Scale bar is 50 nm.

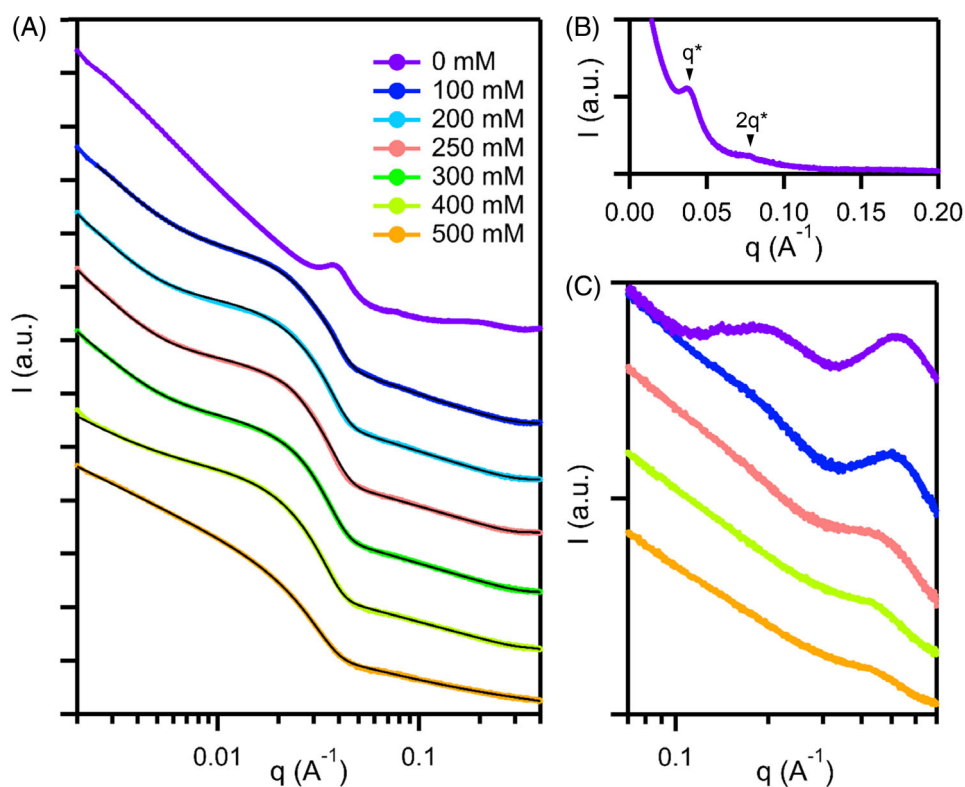
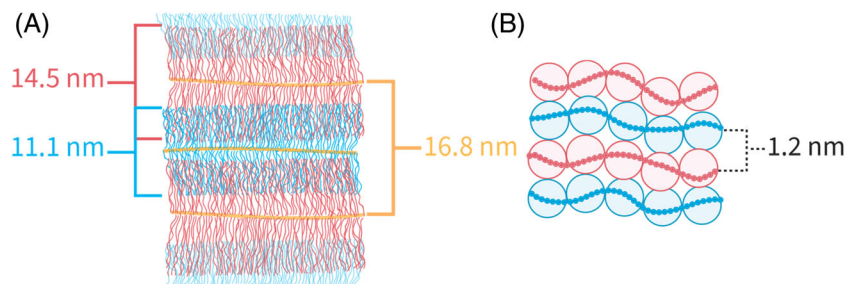


**FIGURE 6** (A) SAXS patterns of bottlebrush polyelectrolyte complexes (BPECs) taken with 0–500 mM NaCl added salt taken at 4 m detector distance. Black lines represent fits from the two-level Beaucage model. (B)  $\log q$  vs  $I$  of a BPEC with 0 mM NaCl and arrows indicating  $q^*$  and  $2q$  (C) High  $q$  SAXS data for BPECs taken at 2.4 m detector distance.

With no added salt,  $I(q)$  scales with  $q^{-3.8}$  at low  $q$ , indicating a mass fractal network with smooth surfaces in good agreement with Cryo-TEM images taken at similar ionic strength. At mid  $q$ , a correlation peak appears at  $q^* \sim 0.0375 \text{ \AA}^{-1}$ , corresponding to an average distance of 16.8 nm. At first, we believed this to be the average distance between PMANa and PTMAEMA bottlebrushes, as correlation peaks arising from bottlebrush–bottlebrush spacings have been reported for solutions of bottlebrush polyelectrolytes and uncharged bottlebrush melts.<sup>36–38</sup> However, this interpretation is inconsistent with observations from the Cryo-TEM images. The average width of a bottlebrush estimated via Cryo-TEM is approximately 13 nm, which means there would need to be around 4 nm of empty space between bottlebrushes

to accommodate a nearly 17 nm inter-bottlebrush distance. We observe densely packed BPEC structures at 0 mM added salt via Cryo-TEM with no evidence gaps between bottlebrushes (Figures 4 and S3). Furthermore, we observe a higher order reflection at  $2q^*$  in the SAXS pattern consistent with lamellar ordering (Figure 6B). Taken together, these results suggest portions of the complex adopt a lamellae-like structures with domain spacing of approximately 17 nm, albeit weakly (Scheme 1A). The domain spacing suggests a significant but incomplete sidechain interpenetration. As the 0 mM salt case presents the strongest driving force for sidechain association, incomplete interpenetration under these conditions suggests sidechain interdigitation is hindered beyond a certain length scale, likely due to steric congestion near the



**SCHEME 1** Illustration of (A) a portion of 0 mM added salt bottlebrush polyelectrolyte complexes (BPEC) aligned in a lamellar fashion in 2D and (B) illustration of sidechain interdigitation and correlation lengths. Bottlebrush widths are estimated via Cryo-TEM, whereas mainchain lamellar spacing and sidechain correlation lengths are estimated via  $q^*$  peak position at mid  $q$  and correlation peak position at high  $q$  in SAXS, respectively.

bottlebrush core. It is possible that improved matching of sidechain lengths and the development of appropriate annealing procedures could drive BPECs toward more well-ordered internal structures and greater sidechain interpenetration at low salt.

With no added salt, we observe scattering from the bottlebrush sidechains as well as two correlation peaks at high  $q$ . Scattering from the two prominent correlation peaks obscures the slope at high  $q$  in this region, making it difficult to estimate sidechain conformations for this salt concentration. The first wide correlation peak at  $q \sim 0.22 \text{ \AA}^{-1}$  we attribute to inter-sidechain distances that are reinforced by steric and electrostatic repulsion in the uncomplexed portions of sidechains, potentially caused by scattering from tightly bound counterions. This correlation peak diminishes quickly upon the addition of salt. We attribute the second correlation peak at  $q \sim 0.53 \text{ \AA}^{-1}$  to the intermolecular spacing of interdigitated bottlebrush sidechains (Scheme 1B). The intensity of this peak diminishes upon the addition of salt and moves to lower  $q$ , changing the sidechain interdigitation spacing from 1.2 to 1.4 nm as salt is added.

Upon the addition of salt, the scattering pattern of BPECs is significantly altered. The most prominent difference is the feature at mid  $q$ . At first, we attempted to model this feature as a flexible cylinder, but efforts to fit the data with this form factor failed to capture the highly negative slope at mid  $q$ . The sharp decreases in intensity where  $I(q)$  scales more negatively than  $q^{-4}$  can arise from diffuse electron density boundaries or polydispersity.<sup>39</sup> As these are mixtures of two structurally distinct bottlebrushes with varying levels of sidechain interpenetration and poorly defined boundaries between species, both factors could be leading to the extremely negative slopes of this feature. To model our data, we applied a shape-independent Beaucage model fit with two levels set to describe the low  $q$  ( $q < 0.01$ ) and high  $q$  ( $q > 0.01$ ) regimes.

The Beaucage model is frequently used to fit SAXS data with a Guinier regime and power law tail, especially when applying an exact scattering model is challenging or impossible.<sup>40,41</sup> The model fits  $R_g$  and a Porod exponent  $P$ . Here, Porod exponents are available for both levels of the fit, whereas  $R_g$  is only apparent at high  $q$  using the  $q$  range available here. Porod exponents allow one to understand how matter is distributed within a material, which we use here to understand network architecture and sidechain conformation.

For fractal objects such as polymers and polymer networks, mass is distributed with respect to distance  $r$  as  $M(r) \sim r^d$  and can be characterized in SAXS via the value of the Porod exponent ( $P$ ) in regions where  $I(q) \sim q^{-P}$ .<sup>42,43</sup> The two primary types of fractals, surface fractals and mass fractals, can be easily distinguished via SAXS. Surface fractals are networks with filled interiors and fractal surfaces, which are indicated by regions where  $I(q)$  decays with Porod exponents of 3–4 and provide the fractal dimension of the surface  $D_s$  through the relationship  $P = 6 - D_s$ . Within a mass fractal, both the structures that compose the network and the surfaces of those structures are fractal. Mass fractals are characterized by Porod exponents of 1–3. Porod exponents closer to 3 represent more collapsed structures, whereas values approaching 1 represent extended structures. In the appropriate  $q$  regime, Porod exponents from scattering data can be related to the Flory exponent ( $\nu$ ) through the relation  $q^{1/\nu} \sim q^{-P}$  to provide a straightforward relationship between scattering data and polymer conformation.<sup>42</sup> The two-level Beaucage model applied here allows us to examine the Porod exponents at low  $q$  (level 1), which we attribute to the network architecture adopted within the BPEC as well as the Porod exponents at high  $q$  (level 2), which we attribute to the sidechain conformation of the bottlebrushes.

The Porod exponent from level 1 (low  $q$ ) fits for 100–300 mM added salt indicate the network adopts as a



surface fractal morphology with a surface slightly rougher than the 0 mM added salt case. Between 300 and 400 mM, a transition from surface fractal to mass fractal occurs, as indicated by a Porod exponent below 3 for the 400 mM sample. At 500 mM, the network adopts an even more expanded conformation with a Porod exponent of 1.84, indicating the network adopts an expanded conformation between that of a polymer in a melt ( $P = 2$ ) and a polymer in a self-avoiding random walk ( $P = 1.7$ ). This network evolution is consistent with the traditional understanding of complex structural development where the addition of salt breaks intrinsic ion pairs, introducing water and swelling the network. The structural development indicated by SAXS agrees well with the BPEC structures observed in Cryo-TEM (Table 1; Figure 4A).

Level 2 (high  $q$ ) allows us to describe the bottlebrushes and their sidechain conformations. In general,

**TABLE 1** Beaucage model fitting results for matched bottlebrush polyelectrolyte complexes.

mM added NaCl	Level 1 ( $q < 0.01$ ) $P$	Level 2 ( $q > 0.01$ )	
		$R_g$	$P$
100	3.48	9.56	1.32
200	3.58	9.93	1.18
250	3.58	9.90	1.08
300	3.30	10.0	1.09
400	2.15	10.8	1.01
500	1.84	9.74	1.00

the  $R_g$  observed here seems to grow slightly with the addition of salt. The sidechains of the bottlebrushes extend as salt is added, evidenced by the decreasing Porod slope at high  $q$  as salt is increased. This is counter-intuitive, as one would expect the sidechains to adopt a more collapsed conformation upon the addition of salt. However, it has also well known that adding salt to a PEC disrupts polymer–polymer ionic interactions in favor of polymer–salt interactions, resulting in a reduction in the relative proportion of complexed regions along a polyelectrolyte chain within a PEC as salt is added. For this reason, we believe chain extension upon the addition of salt suggests a greater thermodynamic penalty for chain collapse in the uncomplexed regions relative to complexed sidechain regions, despite the significant steric congestion in complexed areas.

For the mismatched case, the trends are largely the same with a few significant differences (Figure 7). First, at no added salt, there is little to no evidence of lamellar

**TABLE 2** Beaucage model fitting results for mismatched bottlebrush polyelectrolyte complexes.

mM added NaCl	Level 1 ( $q < 0.01$ ) $P$	Level 2 ( $q > 0.01$ )	
		$R_g$	$P$
100	3.38	8.61	1.6487
200	3.61	8.60	1.33
300	3.04	9.08	1.26
400	1.73	9.77	1.15

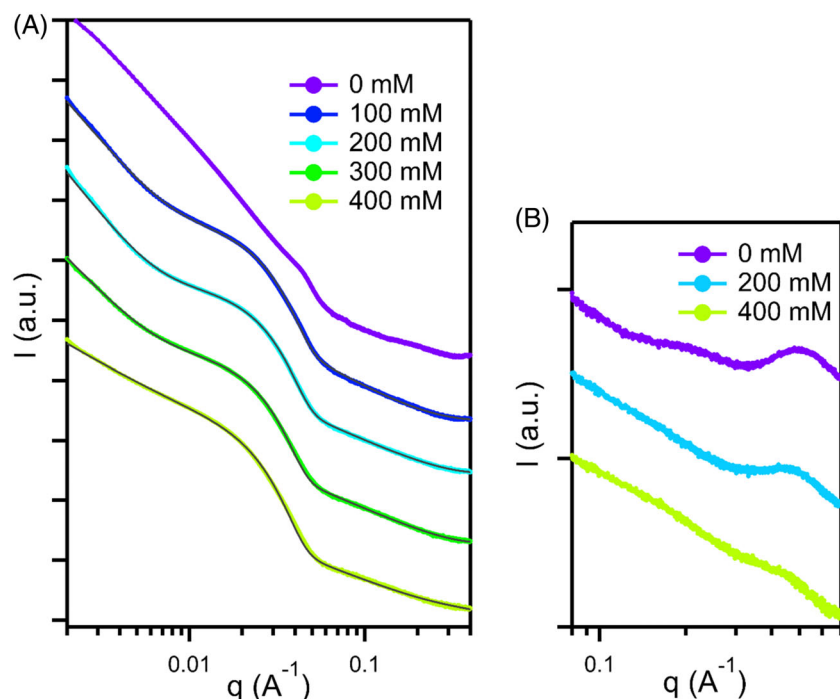


**FIGURE 7** (A) SAXS patterns of mismatched bottlebrush polyelectrolyte complexes (BPECs) taken with 0–500 mM NaCl added salt taken at 4 m detector distance. Black lines represent fits from two-level Beaucage model. (B) High  $q$  SAXS data for BPECs taken at 2.4 m detector distance.



ordering, possibly due to the poorly matched sidechain length hindering the development of ordered structures (Figure 7A). There is a weak correlation peak at  $q \sim 0.045 \text{ \AA}^{-1}$  indicating an average domain spacing of approximately 14.0 nm. Interestingly, the first correlation peak at  $q \sim 0.22 \text{ \AA}^{-1}$  is still present, but much weaker in this sample (Figure 7B). This could be due to the shorter PTMAEMA sidechains being more complexed on average, as PTMAEMA solutions scatter more strongly in this regime than PMANa (Figure S6). Since these samples have much shorter PTMAEMA sidechains, a larger fraction of those sidechains could be available for complexation, leaving fewer uncomplexed sidechains to scatter and contribute to this correlation peak. The peak attributed to intramolecular scattering of bottlebrush sidechains at high  $q$  follows identical trends to the peak found in the matched case, losing intensity, and shifting to lower  $q$  1.2 to 1.4 nm as salt is added.

The fits from the Beaucage model indicate very similar trends to the matched case for 100–400 mM samples. As salt is added, the Porod exponent from high  $q$  fits (level 1) shifts from a surface fractal at 100–300 mM to a mass fractal at 400 mM (Table 2). The  $R_g$ 's for mismatched BPECs are slightly smaller. Interestingly, the Porod exponent is slightly larger than that of the matched case, suggesting that sidechains in this conformation can adopt a more compact conformation relative to those in the matched BPECs. The influence of sidechain length on sidechain conformations within BPECs would benefit from a dedicated study. Mismatched BPEC samples at 500 mM were too soft to handle without disrupting their internal structure, making SAXS measurements infeasible.

### 3 | CONCLUSION

Taken together, our data provide a descriptive picture of the internal structure and material properties of polyelectrolyte complexes composed of oppositely charged bottlebrush polyelectrolytes. We synthesized long and dense branched bottlebrush polymers using a combination of ROMP and ATRP, which we converted into polyelectrolytes using quantitative postpolymerization modification. Bottlebrush polyelectrolyte complexes of PMANa and PTMAEMA bottlebrushes form white solids that behave mechanically as gels that soften with added salt, increased heat and greater sidechain mismatching. Cryo-TEM reveals significant interpenetration between bottlebrushes that could act as joints in the network as it expands. We hypothesize that these joints act as physical crosslinks that restrict polymer motion, leading to gel-like mechanical response. As salt or temperature is

increased, the density of the joints decreases, leading to gels with lower moduli. Cryo-TEM images and SAXS data reinforce each other to provide a cohesive model of the BPEC structural development upon the addition of salt. Bottlebrush polyelectrolyte complexes at low salt are densely packed surface fractal networks with internal domain spacings of  $\sim 17$  nm and smooth surfaces that expand upon the addition of salt. Between 300 and 400 mM added NaCl, the network becomes a mass fractal, which expands upon the addition of salt until dissolving above 500 mM. Sidechains expand as salt is added, suggesting that sections of the sidechain in interdigitated regions of the BPECs are more collapsed than sidechain portions within uncomplexed regions of BPECs. Our results develop a fundamental understanding of the structure and properties of polyelectrolyte complexes composed of bottlebrush polyelectrolytes, enabling future investigation into the mechanical and structural variation attainable by incorporating branched polyelectrolytes into PEC design.

### ACKNOWLEDGMENTS

Parts of this work were carried out at the Soft Matter Characterization Facility of the University of Chicago. The authors would like to thank Dr. Tera Lavoie from The University of Chicago Advanced Electron Microscopy Core Facility for assistance with Cryo-TEM, and Dr. Xiaobing Zuo, Elina Ghmire and Charlie Lindberg for assistance collecting SAXS data at Argonne National Laboratory Advanced Photon Source beamline 12-ID-B. This work used resources of the Advanced Photon Source, a U.S. Department of Energy (DOE) Office of Science User Facility operated for the DOE Office of Science by Argonne National Laboratory under Contract no. DE-AC02-06CH11357.

### FUNDING INFORMATION


This work was supported by the Division of Materials Science and Engineering, Basic Energy Sciences, Office of Science, U.S. Department of Energy. This work made use of the shared facilities at the University of Chicago Materials Research Science and Engineering Center, supported by National Science Foundation under award number DMR-2011854.

### CONFLICT OF INTEREST STATEMENT

The authors declare no competing financial interest.

### ORCID

Kaden C. Stevens  <https://orcid.org/0000-0002-5853-8765>

Matthew V. Tirrell  <https://orcid.org/0000-0001-6185-119X>

## REFERENCES

- [1] L. Li, A. M. Rumyantsev, S. Srivastava, S. Meng, J. J. de Pablo, M. V. Tirrell, *Macromolecules* **2020**, *54*, 105.
- [2] L. Li, S. Srivastava, M. Andreev, A. B. Marciel, J. J. de Pablo, M. V. Tirrell, *Macromolecules* **2018**, *51*, 2988.
- [3] M. Muthukumar, *Macromolecules* **2017**, *50*, 9528.
- [4] C. E. Sing, S. L. Perry, *Soft Matter* **2020**, *16*, 2885.
- [5] S. Srivastava, M. V. Tirrell, in *Advances in Chemical Physics*, Vol. 161 (Eds: S. A. Rice, A. R. Dinner), John Wiley & Sons, Inc., Hoboken, NJ **2016**, p. 499.
- [6] J. Van der Gucht, E. Spruijt, M. Lemmers, M. A. C. Stuart, *J. Colloid Interface Sci.* **2011**, *361*, 407.
- [7] M. Lueckheide, J. R. Vieregge, A. J. Bologna, L. Leon, M. V. Tirrell, *Nano Lett.* **2018**, *18*, 7111.
- [8] W. C. Blocher, S. L. Perry, *Wiley Interdiscip. Rev. Nanomed. Nanobiotechnol.* **2017**, *9*, e1442.
- [9] I. K. Voets, A. de Keizer, M. A. Cohen Stuart, *Adv. Colloid Interface Sci.* **2009**, *147-148*, 300.
- [10] D. Peters, M. Kastantin, V. R. Kotamraju, P. P. Karmali, K. Gujraty, M. Tirrell, E. Ruoslahti, *Proc. Natl. Acad. Sci. U.S.A.* **2009**, *106*, 9815.
- [11] S. Lindhoud, W. Norde, M. A. Cohen Stuart, *Langmuir* **2010**, *26*, 9802.
- [12] F. Maggi, S. Ciccirelli, M. Diociaiuti, S. Casciardi, G. Masci, *Biomacromolecules* **2011**, *12*, 3499.
- [13] Q. Zhao, D. W. Lee, B. K. Ahn, S. Seo, Y. Kaufman, J. N. Israelachvili, J. H. Waite, *Nat. Mater.* **2016**, *15*, 407.
- [14] I. A. van Hees, A. H. Hofman, M. Dompé, J. van der Gucht, M. Kamperman, *Eur. Polym. J.* **2020**, *141*, 110034.
- [15] Z. Zhou, C.-F. Yeh, M. Mellas, M.-J. Oh, J. Zhu, J. Li, R.-T. Huang, D. L. Harrison, T.-P. Shentu, D. Wu, *Proc. Natl. Acad. Sci. U.S.A.* **2021**, *118*, e2114842118.
- [16] Q. Wang, J. B. Schlenoff, *Macromolecules* **2014**, *47*, 3108.
- [17] S. Meng, J. M. Ting, H. Wu, M. V. Tirrell, *Macromolecules* **2020**, *53*, 7944.
- [18] A. E. Smith, X. Xu, C. L. McCormick, *Prog. Polym. Sci.* **2010**, *35*, 45.
- [19] A. W. York, S. E. Kirkland, C. L. McCormick, *Adv. Drug Deliver. Rev.* **2008**, *60*, 1018.
- [20] A. E. Marras, J. M. Ting, K. C. Stevens, M. V. Tirrell, *J. Phys. Chem. B.* **2021**, *125*, 7076.
- [21] D. V. Krogstad, N. A. Lynd, S. H. Choi, J. M. Spruell, C. J. Hawker, E. J. Kramer, M. V. Tirrell, *Macromolecules* **2013**, *46*, 1512.
- [22] D. V. Krogstad, N. A. Lynd, D. Miyajima, J. Gopez, C. J. Hawker, E. J. Kramer, M. V. Tirrell, *Macromolecules* **2014**, *47*, 8026.
- [23] J. Huang, F. J. Morin, J. E. Laaser, *Macromolecules* **2019**, *52*, 4957.
- [24] M. Yang, J. Shi, J. B. Schlenoff, *Macromolecules* **2019**, *52*, 1930.
- [25] K. Akkaoui, M. Yang, Z. A. Digby, J. B. Schlenoff, *Macromolecules* **2020**, *53*, 4234.
- [26] J. Huang, J. E. Laaser, *ACS Macro Lett.* **2021**, *10*, 1029.
- [27] A. M. Rumyantsev, N. E. Jackson, B. Yu, J. M. Ting, W. Chen, M. V. Tirrell, J. J. De Pablo, *ACS Macro Lett.* **2019**, *8*, 1296.
- [28] B. M. Johnston, C. W. Johnston, R. A. Letteri, T. K. Lytle, C. E. Sing, T. Emrick, S. L. Perry, *Org. Biomol. Chem.* **2017**, *15*, 7630.
- [29] Y. Yamauchi, N. N. Horimoto, K. Yamada, Y. Matsushita, M. Takeuchi, Y. Ishida, *Am. Ethnol.* **2021**, *133*, 1552.
- [30] F. A. Plamper, M. Ruppel, A. Schmalz, O. Borisov, M. Ballauff, A. H. E. Müller, *Macromolecules* **2007**, *40*, 8361.
- [31] F. A. Plamper, H. Becker, M. Lanzendörfer, M. Patel, A. Wittemann, M. Ballauff, A. H. E. Müller, *Macromol. Chem. Phys.* **2005**, *206*, 1813.
- [32] Y. Liu, B. Momani, H. H. Winter, S. L. Perry, *Soft Matter* **2017**, *13*, 7332.
- [33] M. Yang, S. L. Sonawane, Z. A. Digby, J. G. Park, J. B. Schlenoff, *Macromolecules* **2022**, *55*, 7594.
- [34] Y. Liu, C. F. Santa Chalarca, R. N. Carmean, R. A. Olson, J. Madinya, B. S. Sumerlin, C. E. Sing, T. Emrick, S. L. Perry, *Macromolecules* **2020**, *53*, 7851.
- [35] E. Spruijt, M. A. Cohen Stuart, J. van der Gucht, *Macromolecules* **2013**, *46*, 1633.
- [36] J. M. Sarapas, T. B. Martin, A. Chremos, J. F. Douglas, K. L. Beers, *Proc. Natl. Acad. Sci. U.S.A.* **2020**, *117*, 5168.
- [37] F. Horkay, A. Chremos, J. F. Douglas, R. L. Jones, J. Lou, Y. Xia, *J. Chem. Phys.* **2020**, *152*, 194904.
- [38] F. Horkay, A. Chremos, J. F. Douglas, R. Jones, J. Lou, Y. Xia, *J. Chem. Phys.* **2021**, *155*, 074901.
- [39] A. Yildirim, K. Sentker, G. J. Smales, B. R. Pauw, P. Huber, A. Schönhals, *Nanoscale Adv.* **2019**, *1*, 1104.
- [40] H. Wu, J. M. Ting, O. Werba, S. Meng, M. V. Tirrell, *J. Chem. Phys.* **2018**, *149*, 163330.
- [41] G. Beaucage, *J. Appl. Crystallogr.* **1995**, *28*, 717.
- [42] E. M. Anitas, *Complexity in Biological and Physical Systems*, BoD – Books on Demand, Norderstedt, Germany **2018**, p. 169.
- [43] M. Rubinstein, R. H. Colby, *Polymer Physics*, Oxford University Press, New York **2003**.

## SUPPORTING INFORMATION

Additional supporting information can be found online in the Supporting Information section at the end of this article.

**How to cite this article:** K. C. Stevens, M. V. Tirrell, *J. Polym. Sci.* **2023**, *1*. <https://doi.org/10.1002/pol.20230540>